Unsupported SiO_2-based organic–inorganic membranes
Part 1.—Synthesis and structural characterization

Sandra Dirè,*[a] Eva Pagani,[a] Florence Babonneau,[b] Riccardo Ceccato[a] and Giovanni Carturan[a]

[a]*Dipartimento di Ingegneria dei Materiali, Università di Trento, v. Mesiano 77, 38050 Trento, Italy*

[b]*Chimie de la Matière Condensée, Université Pierre et Marie Curie/CNRS, 4, place Jussieu, Paris, France*

Tetraethoxysilane (TEOS) and methyltriethoxysilane (MTES) have been used to prepare hybrid SiO_2-based membranes. These self-supported materials were obtained from controlled polymerization reactions for various TEOS/MTES molar ratios ensuring the achievement of crack-free disks 8 cm in diameter and 10–40 μm in thickness. The rheological behaviour of precursor solutions was studied and gelling times were determined. The whole process, from starting solution to xerogel, was followed by FTIR spectroscopy, viscosity measurements and multinuclear solid-state NMR, and is discussed in terms of the hydrolysis–condensation kinetics of tetrafunctional and trifunctional silicon alkoxides. Density, shrinkage, elastic modulus (E), modulus of rupture (MOR) and elongation at break were all determined and related to preferential structural arrangements of networks according to the TEOS/MTES ratio.

Hybrid organic–inorganic materials are currently under investigation as potential multifunctional and high-performance materials: organic modified ceramics (ORMOCERs) properties are exploited in the fields of adhesives, sealing and modified glass surface materials,[1–3] sensors[4] and artificial membranes.[5–8]

As regards membrane technology, the extension of application fields to more and more sophisticated processes parallels the development of the new class of inorganic membranes, which can also compete with organic polymers in terms of chemical and thermal durability and separation performances. Sensors and membranes are involved with mass transport phenomena due to concentration, pressure or electrical field gradients: any chemical modification causing changes of network structure and surface features affects detection or separation properties so that hybrid materials are expected to improve the development of inorganic membranes.

The sol–gel process can lead easily to silica-based hybrid materials containing Si—O and Si—C bonds: intrinsic molecular gels with both organic and inorganic moieties are obtained by using $R'_nSi(OR)_{4-n}$ as precursors.[9–11] Note that the conditions chosen for hydrolysis–condensation of these precursors affect the structural features and physical properties of the final products.[12,13] Obviously, with a constant CH_3/Si/O ratio, the ordinary synthesis of hybrid SiO_2 materials, from mixtures of $Si(OR)_4$, as cross-linking agent and di- or tri-functional methylsilanes, may not lead to the same product as that obtained from pure $CH_3Si(OR)_3$; in particular, the different spatial location of CH_3—Si bonds may result in different porosities and pore size distributions. This apparent complication may modify mechanical properties: in particular, concentration and distribution of CH_3—Si groups may influence the achievement of self-carrying items.

In this initial work, the sol–gel process was used to prepare self-supported, hybrid organic–inorganic membranes from mixtures of silicon tetraalkoxide and $CH_3Si(OEt)_3$: results on the development of the gel structure from these precursors and on the characterization of the resulting xerogels with various $Si(OEt)_4/CH_3Si(OEt)_3$ ratios, will be presented in this paper, while gas-separation properties and surface characterization will be reported in a future paper.

Experimental

Synthesis of $Si(OEt)_4$/$MeSi(OEt)_3$ gels

Various mixtures of $Si(OEt)_4$ (TEOS) and $CH_3Si(OEt)_3$ (MTES) were hydrolysed at room temperature with an HCl solution at pH = 1.5. Various water/alkoxide ratios were calculated for the different compositions, so that $H_2O/SiOEt = 0.5$. No solvent was used except for the pure $Si(OEt)_4$ gel (ethanol). Details concerning the labelling of samples, compositions and preparation conditions are reported in Table 1.

Solutions were stirred at room temperature, using storage times determined by solution rheology, affected by the TEOS/MTES ratio. Each solution (2.4 ml) poured into polystyrene Petri dishes (diameter 8 cm) and covered by polymer foil afforded clear, homogeneous gel membranes in *ca.* 10 days, during which time several pinholes on the foil were made. Samples of thickness 10–40 μm were allowed to dry in air at constant temperature and humidity (Fig. 1).

Characterization techniques

The rheological properties of the gelling solutions were determined at 24.8 ± 0.2 °C with a cone/plate system using a MC-10 Physica viscosimeter. Values of shear stress, shear rate, temperature and viscosity were collected for the various solutions during ageing.

Solid-state NMR measurements were performed on a MSL 400 Bruker spectrometer. Solid samples were spun at 4 kHz. For the ^{29}Si single-pulse experiments (SPE), pulse width (2 μs: $\theta = 30°$) and relaxation delays (30 s) were chosen to take into account the long T_1 relaxation times. ^{29}Si MAS NMR spectra were also recorded using cross polarization (CP) techniques and variable contact times. The spectra were analysed using the WINNMR and WINFIT programs.[14] ^{13}C CP MAS NMR spectra were recorded using 2 ms contact time. Recycle delays of 10 s were used for all CP spectra.

FTIR spectra were recorded on a Nicolet 5DXC instrument equipped with both horizontal attenuated total reflectance (HATR) and diffuse reflectance (DR) accessories. In the HATR mode, a known volume of sol was poured directly onto the surface of the ZnSe crystal, closed with an appropriate cap; 64 scans at 45° to the IR incident radiation were collected. For DR measurements, xerogels were powdered and dispersed in KBr, accumulating 64 scans for each spectrum.

Densities were measured in water and hexane at 25 °C by Archimedes' method; linear shrinkage was calculated by measuring the xerogels' diameters and expressing them as percentages referring to the Petri dish diameter. MOR, Young's modulus (E) and maximum elongation at break (ε_R) were obtained with a three-point bending test, using an Instrom

Table 1 Sample labels and compositions

Sample label, TxMy	composition, molar ratio	H_2O/Si molar ratio	ethanol/Si molar ratio	$[Si]_0$/mol l^{-1}
T100	100 TEOS	2	0.5	3.47
T70M30	70 TEOS/30 MTES	1.85	—	4.01
T50M50	50 TEOS/50 MTES	1.75	—	4.12
T30M70	30 TEOS/70 MTES	1.65	—	4.24
M100	100 MTES	1.5	—	4.42

Fig. 1 T70M30 xerogel disk

testing machine with a load cell of 100 N and a testing rate of 1 mm min^{-1}.

Results

The hydrolysis and condensation process of MTES and TEOS precursors at various ratios was studied using different techniques, in order to compare the advance of the gelling process and of the gel network structure.

IR spectra

Fig. 2(*a*) shows FTIR spectra recorded in the HATR mode in the interval 4000–650 cm^{-1} for T100, T50M50 and M100 samples, 15 min after preparation of the solutions. In the high-frequency field, C—H stretching vibrations at 3000–2850 cm^{-1} and a wide band centred at 3350 cm^{-1} due to O—H stretching were present. The bending vibrations of the Et and Me groups were observed in the interval 1500–1300 cm^{-1}; for compositions containing MTES, a precise signal due to Si—CH_3 stretching was recorded at 1276 cm^{-1}. The 1200–1000 cm^{-1} region showed overlapping signals of O—Si—O bonds in different species. The signal due to Si—OEt bonds at 954 cm^{-1} was recognized clearly in the T100 spectrum, absorption due to ethanol being observed at 880 cm^{-1}; the M100 spectrum displays peaks at 916 cm^{-1} attributed to Si—OH and Si—O^- bonds,[15] and that of ethanol at 880 cm^{-1}. The signal at 955 cm^{-1} was virtually lost, suggesting that the hydrolysis of ethoxide groups in this sample was almost completed. In the T50M50 spectrum, an intermediate situation appeared with peaks at 955, 920 and 880 cm^{-1}. Spectra recorded after 120 min are shown in Fig. 2(*b*). In the T100 sample, the band at 3350 cm^{-1} revealed large amounts of water and ethanol, which decreased as the MTES content increased, in agreement with a decrease of the signal at 1637 cm^{-1} [δ(OH)]. The M100 sample was characterized by almost complete hydrolysis, the Si—CH_3 signal at 1276 cm^{-1} and the Si—OH one at 916 cm^{-1} still being visible. Instead, a remarkable concentration of Si—OEt was observed in T100, while T50M50 showed intermediate behaviour. The M100 spectrum recorded between 120 min and gelling time (220 min) remained virtually unchanged, whereas slow, progressive evolution was found for

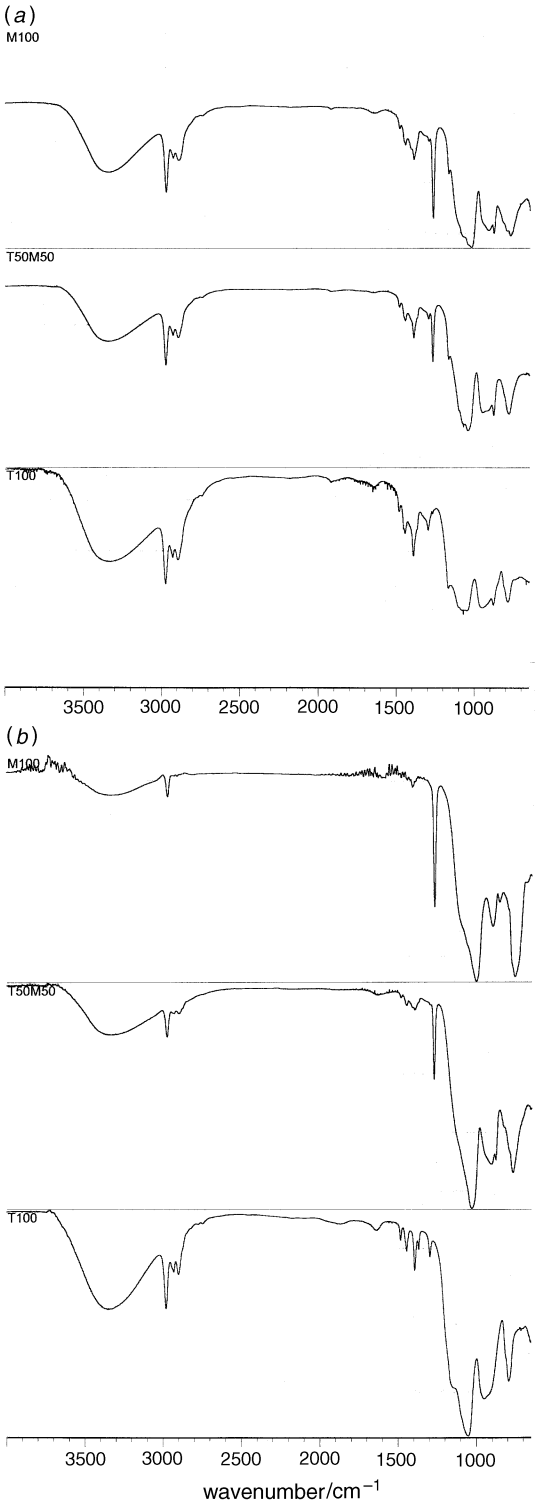

Fig. 2 HATR-FTIR spectra recorded (*a*) 15 min and (*b*) 120 min after preparation of the T100, T50M50 and M100 sols

T100 in the interval 120–330 min, *i.e.* T100 gelling time. This supports the fact that hydrolysis–condensation processes still occur for T100 when the MTES sample had already gelled.

Fig. 3 reports 4000–400 cm^{-1} spectra recorded in the DR mode, which revealed the spectral window between 650 and 400 cm^{-1}. T*x*M*y* films, stored at the same temperature and humidity, show that adsorbed water increased as %TEOS increased (bands at 3300 and 1630 cm^{-1}). In the 3000–2800 cm^{-1} interval, C—H stretching vibrations of residual OEt and Me groups were present; the intensity of the peak at 1272 cm^{-1} [$\nu(Si-CH_3)$] decreased as the MTES concentration decreased. Other features were the intensity inversion of peaks in the 1200–1000 cm^{-1} interval and the lowering of the peak at 940 cm^{-1} (Si—OH and Si—OEt) as the amount of MTES increased. The position of the peak corresponding to the angular deformation δ(Si—O—Si) and related to the silica units arrangement,[16] at 466 cm^{-1} in the T100 spectrum, was shifted to lower frequencies as %MTES increased.

Viscosity measurements

Fig. 4 reports the evolution of solution viscosities of the T*x*M*y* samples. Viscosity *vs.* time diagrams indicate a relationship between the viscosity increase and composition; samples with higher concentrations of MTES displayed a viscosity increase at 238–250 min ageing time, whereas TEOS-rich compositions showed a net increase after 327–342 min, the slope of the curve being appreciably smaller. A trend discontinuity was observed for T30M70, whose transition occurred at 226 min.

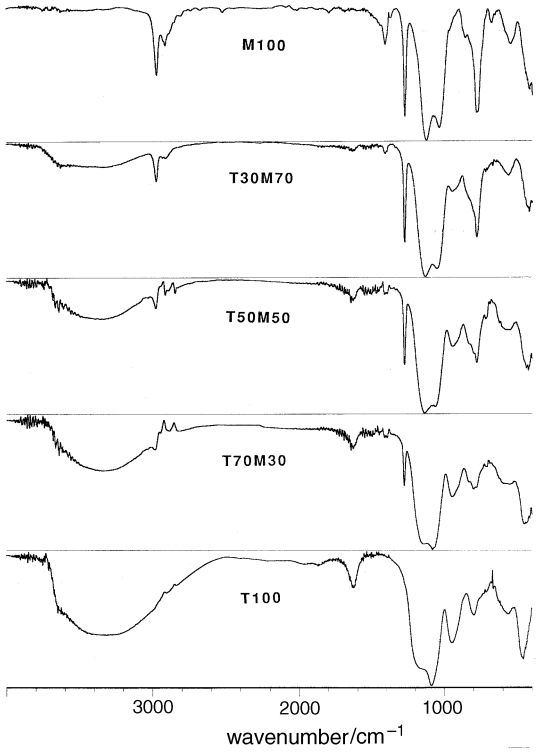

Fig. 3 DRIFT spectra of the T*x*M*y* xerogels

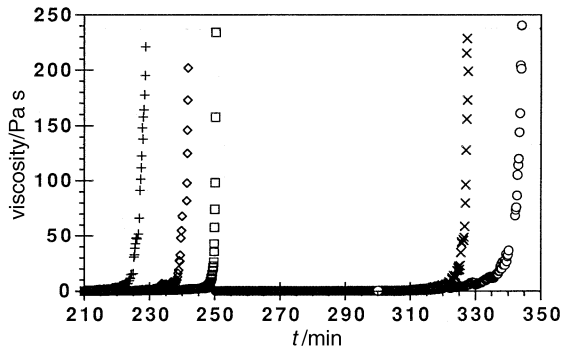

Fig. 4 Viscosity *vs.* time diagrams of the T*x*M*y* samples: ◇, M100; ○, T100; □, T50M50; +, T30M70; ×, T70M30

Shear stress *vs.* shear rate and viscosity *vs.* shear rate plots are shown in Fig. 5. M100 lost Newtonian flow behaviour after 200 min [Fig. 5(*a*)], while T100 showed it up to 305 min [Fig. 5(*b*)]; in both cases, further ageing produced yield behaviour [Fig. 5(*c*) and (*d*)].[17] T*x*M*y* compositions displayed intermediate behaviour.

NMR results

Solid-state NMR (MAS NMR) can provide direct information on the local environment of different structural units, and thus on the degree of condensation of the network. Fig. 6 shows the ^{29}Si MAS NMR spectra of T100, T50M50 and M100 recorded as single-pulse experiments (SPE); Table 2 shows the percentages of various units obtained after simulation of SPE spectra, as well as the degree of condensation of the network. It confirms what was published previously,[18] that the degree of condensation decreases with the average functionality of the precursors. It is interesting to note that the degree of condensation of the T50M50 sample is intermediate between those of the T100 and M100 samples.

Series of ^{29}Si CP MAS NMR spectra with variable contact times were also recorded on the three samples. Analysis of the variation of magnetization *vs.* contact time was carried out according to the simplest model describing CP between two spin reservoirs, one for dilute spins, S, and one for abundant spins, I, using the well known formula:[19]

$$M_S(t_c)=\frac{\gamma_I}{\gamma_S}M_{0S}\frac{1}{1-\lambda}\left\{1-\exp\left[-(1-\lambda)\frac{t_c}{T_{IS}}\right]\right\}\exp\left(-\frac{t_c}{T_{1\rho}{}^I}\right)$$

with $\lambda = T_{IS}/T_{1\rho}{}^I$. M_{0S} is the magnetization at the equilibrium in the static field B_0, T_{IS} is the CP standard time which is related to the strength of the I–S dipolar coupling and $T_{1\rho}{}^I$ is the relaxation time of the abundant spins in the rotating frame, which will cause a loss of magnetization for long contact time. γ_I and γ_S are the magnetogyric ratios for spins I and S, respectively. This formula applies for S spins which are partially decoupled from the protons. The T_{SiH} and $T_{1\rho}{}^H$ fitted values are reported in Table 2 as well as the percentages of the various units detected by CP, and estimated from the M_{0S} value. For T100 and M100 samples, the agreement factor for the fitting procedure, R, is > 0.99, showing a good agreement between the experimental behaviour and the theoretical model. In the case of the T50M50 CP MAS spectrum, a lower agreement factor is obtained ($R > 0.97$) which may be related to the presence of several local environments for the different T and Q sites.

Two interesting features can be pointed out from this study. First, a comparison between the quantitative analyses of the various sites carried out from the SPE and CP spectra shows perfect agreement for the M100 and T50M50 samples, and a discrepancy for the T100 sample. In this last sample, the number of Q_4 units is underestimated in the CP technique, suggesting that the analysis of the CP dynamics measures only the amount of Q_4 units close to Q_3 or Q_2 units. In contrast, in the T50M50 system, the Q_4 units should be in close proximity to T units, which allows their detection *via* the CP technique. A second interesting point is the difference in the T_{SiH} values corresponding to the Q units, in the T100 and T50M50 samples. Their decrease in the T50M50 sample indicates stronger ^1H–^{29}Si dipolar coupling for these units and could be related to the close proximity of the T units. These results strongly suggest a good chemical homogeneity of the T and Q units within the T50M50 sample.

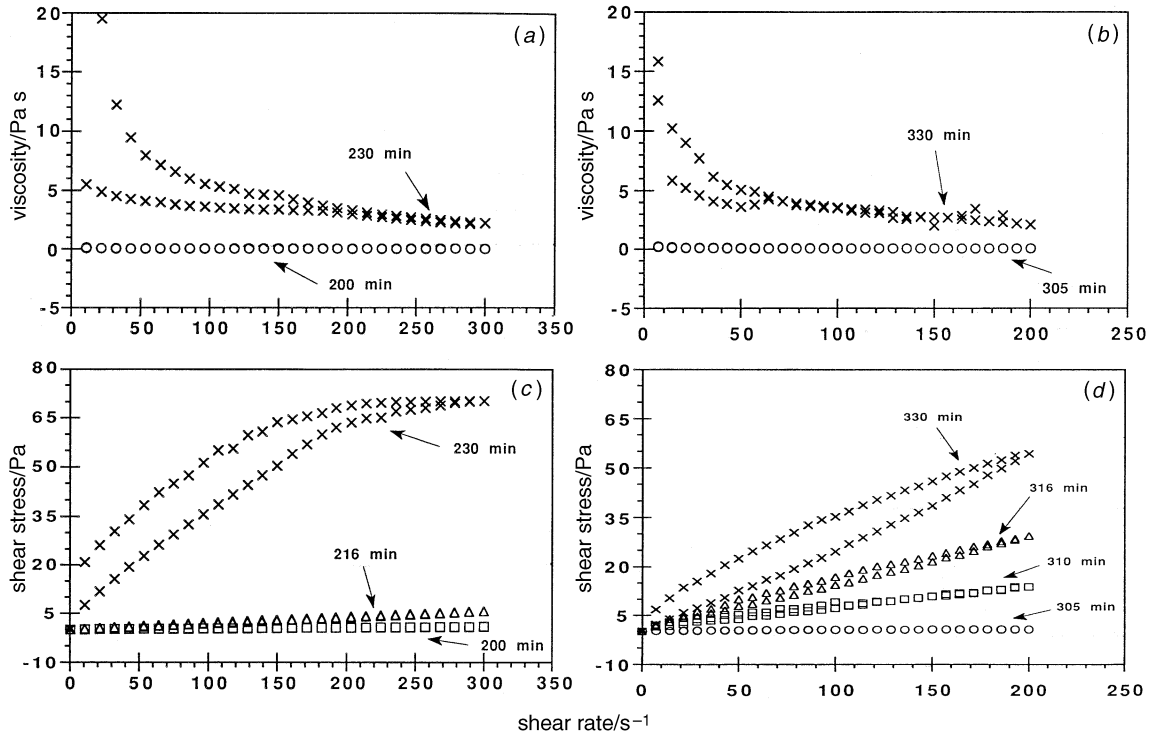

Fig. 5 Viscosity *vs.* shear rate [(*a*) and (*b*)] and shear stress *vs.* shear rate [(*c*) and (*d*)] plots of M100 [(*a*) and (*c*)] and T100 [(*b*) and (*d*)] samples

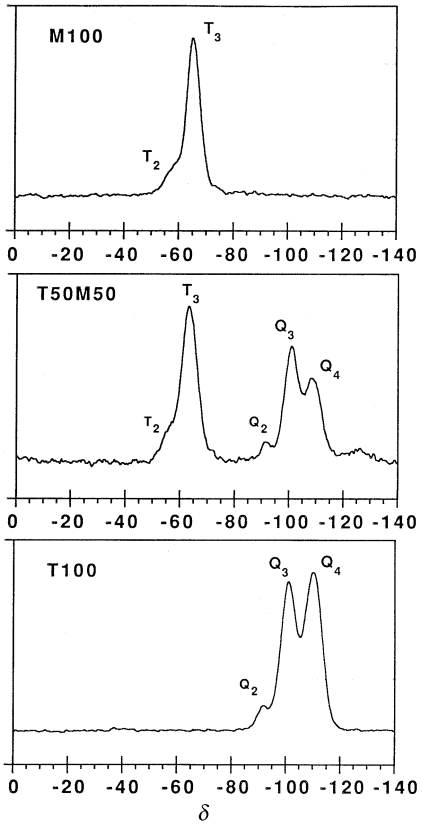

Fig. 6 ^{29}Si MAS NMR spectra of M100, T50M50 and T100 xerogels

^{13}C CP MAS NMR and ^{1}H MAS NMR spectra (Fig. 7), recorded on M100 and T50M50 samples, show the presence of Si—Me groups with signals at δ −3.7 and 0.4, respectively. Moreover, these spectra indicate an incomplete hydrolysis–condensation process. As a matter of fact, the signals due to residual Si—OEt groups are present in the ^{13}C CP MAS NMR spectra (δ 18.4 and 58.1 for M100, δ 17.6 and 59.9 for T50M50), and a signal attributed to Si—OH terminal units (δ 4.1) is present in the ^{1}H MAS NMR spectrum of the T50M50 xerogel [Fig. 7(*b*)].

Physical and mechanical results

The density, shrinkage and mechanical features of the xerogel membranes were also studied. Densities are reported in Table 3; a linear decrease as the percentage of MTES increased was observed. Shrinkages, calculated as described in the Experimental section, displayed a linear relationship with MTES content (Fig. 8), proving the absence of linear shrinkage for M100.

Mechanical measurements performed on thin bars of the xerogel were obtained by a three-point bending test; the results are reported in Table 4. The elastic modulus, E, is an intrinsic property depending on the bond density and related to the material structure. The E value of T100 agrees with reported values of silica xerogels prepared under acidic conditions, *i.e.* 5–10 GPa.[20] The decrease in elastic modulus as the organic load increased accounted for the lower cross-linking consequent upon the introduction of a trifunctional precursor. The consequent reduction in Si—O bond density also affected the maximum elongation at break ε_R, which increased with MTES concentration. Fracture surfaces were featureless and disks appeared dense and macroscopically homogeneous, as shown in Fig. 9.

Discussion

For a two-step acid–base process, van Bommel *et al.*[21] reported that, under acidic and neutral conditions, the hydrolysis rate of alkyl-substituted silicon alkoxides is faster than for TEOS; moreover, condensation already occurs in the acid step. These observations have been confirmed recently:[22a] after the addition of water, under acidic conditions, the hydrolysis of alkyl-substituted alkoxides with short alkyl chains is almost complete within the first few minutes and the condensation degree increases quickly during the first 2 h and then slows.

Results obtained for T*x*M*y* samples are consistent with these works, based on viscosity and NMR results:[21,22] the HATR-FTIR spectra indicate that MTES is hydrolysed faster than

Table 2 ^{29}Si solid-state NMR data

sample	site[a]	δ	T_{SiH}/ms	$T_{1\rho}$/ms	units obtained (%) SPE	CP	degree of condensation
M100	T_3	−65.2	1.7	52	88	86	0.96
	T_2	−57.6	1.1	48	12	14	
T100	Q_4	−110.9	8.7	82	49	25	
	Q_3	−101.4	4.2	27	44	64	0.85
	Q_2	−92.1	3.6	21	7	11	
T50M50	T_3	−63.1	2.2	123	45	42	
	T_2	−55.3	1.6	70	5	10	
	Q_4	−108.9	5.1	177	21	20	0.89
	Q_3	−100.7	2.2	113	25	25	
	Q_2	−91.7	1.5	65	4	3	

[a] T_n and Q_n: n = number of bridging oxygens.

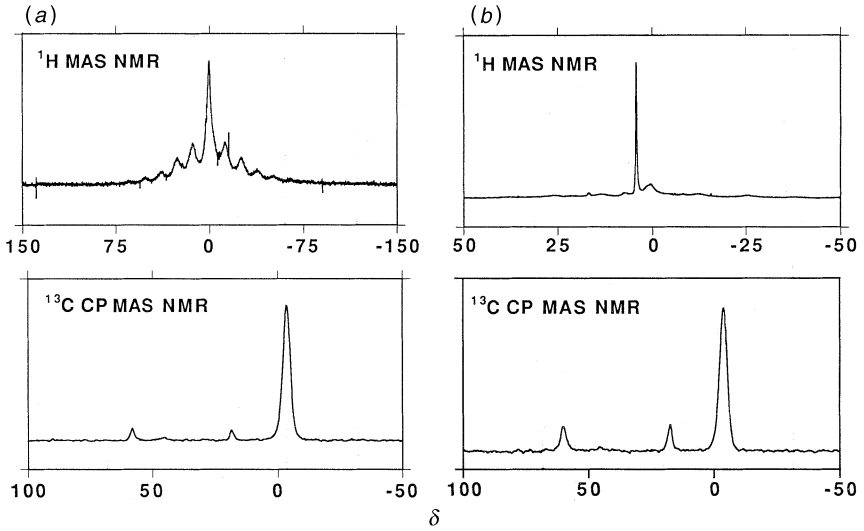

Fig. 7 ^{1}H MAS NMR and ^{13}C CP MAS NMR spectra of (a) M100 and (b) T50M50 xerogels

Table 3 T*x*M*y* density results

sample	density/g cm^{-3}
T100	1.84±0.04
T70M30	1.61±0.03
T50M50	1.48±0.02
T30M70	1.34±0.04
M100	1.29±0.05

Table 4 Mechanical characterization of T*x*M*y* samples

sample	E/GPa	ε_R (%)	MOR (MPa)
T100	5.2±0.6	7	40±10
T50M50	2.6±0.3	19	50±8
M100	0.7±0.1	43	30±10

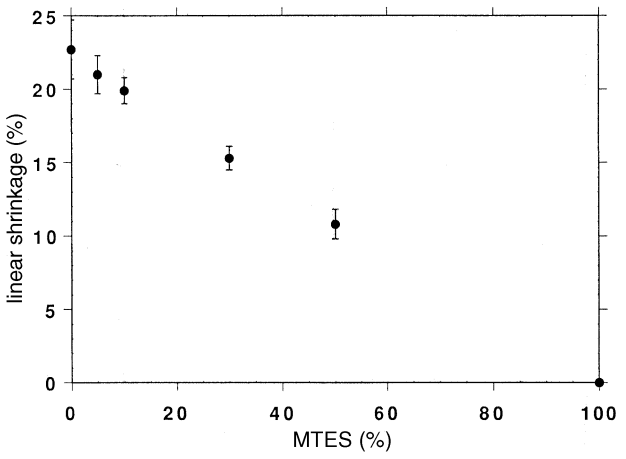

Fig. 8 Linear shrinkage *vs.* %MTES of T*x*M*y* disks

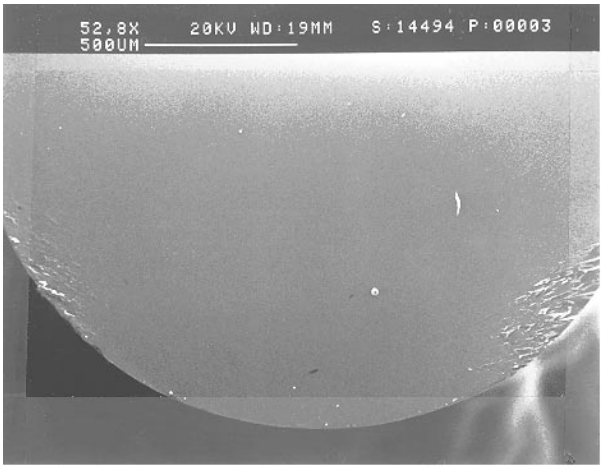

Fig. 9 Fracture surface of the T50M50 bar (SEM image)

TEOS, since the concentration of ethoxy groups for M100 is reduced markedly after 15 min; moreover, hydrolysis seems to be complete in 120 min, and extensive condensation of silanols may be deduced from the negligible evolution of the M100 spectra from 120 min to gelling time. The different behaviour in the reactivities of M100 and T100 under acidic conditions may be ascribed to the inductive effect of the CH_3 group, leading to activated species **1** which is lower in energy than **2**, ultimately resulting in faster hydrolysis–condensation reactions for MTES.[23]

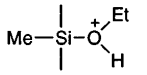

1

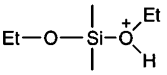

2

This interpretation is consistent with the short time required for M100 viscosity increase. The fast condensation reaction leads to extended oligomers, which collapse to the gel network by condensation of few residual Si—OH bonds: indeed, the gelling time of M100 is shorter than that of T100, in which the viscosity increase takes much longer, suggesting slower, continuous Si—OH condensation.[17] The gelling kinetics for M100 and T100 solutions having intermediate compositions do not lead to behaviours corresponding to the sum of M100 and T100 behaviours multiplied by the molar fractions of relevant precursors: for instance, the viscosity trend of T50M50 is very close to that of M100 (Fig. 4). This observation deserves some specific comments. If gelling time is considered as a kinetic parameter which substantiates the occurrence of a closed SiO_2 network, *i.e.* the occurrence of a structure where most oxygens bridge two Si atoms, parameter τ, defined as:

$$\tau = \frac{\text{Si functionality}}{\text{gelling time}}[\text{Si}]_0$$

where $[\text{Si}]_0$ = silicon concentration in the starting solutions (Table 1), Si functionality = number of Si—OR in the starting precursor, quantifies the rate required for engaging the Si—O bonds of the precursors in Si—O—Si units per volume unit. Values of τ for each sample are shown in Fig. 10 *vs.* MTES mol%. Clearly, MTES accelerates the occurrence of the gel; in fact τ increases above the value expected if the process resulted from the sum of the individual gelling processes of TEOS and MTES (Fig. 10, dotted line). From the viewpoint of reaction mechanism, this fact implies that terminal Si—OH groups derived from TEOS are involved more rapidly in condensation to Si—O—Si upon reaction with Si—OH groups derived from MTES. Indeed, partial cocondensation between T and Q units may be presumed in the T50M50 gel, considering the variations in T_{SiH} of T and Q units compared to T100 (Q) and M100 (T) gels (Table 2) and the lower agreement factor between the experimental and simulated spectra. The decrease in T_{SiH} of Q units in T50M50, compared also with results reported for silica gels prepared from TEOS in acid conditions,[24] could be ascribed to the formation of an intimate mixture between silica gel and organic modified moieties.[25] T_{SiH} values of 1 ms have been reported for T units in which the Si atom is surrounded by three bridging oxygens.[26] The slight increase in T_{SiH} of T units in T50M50, owing to a low effectiveness of magnetization transfer for short contact times, could be related to a different mobility of T units in the network.

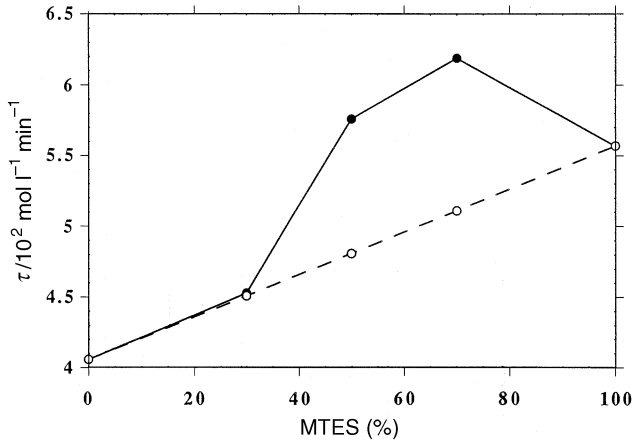

Fig. 10 Parameter τ *vs.* MTES mol(%) (τ = Si functionality $\times [\text{Si}]_0$/gelling time) [●, experimental; ○, calculated (mixture rule)]

Peeters *et al.*[27] recently studied the functionality of hybrid gels obtained from mixtures of TEOS and various trifunctional organosilanes and concluded that, in spite of the enhanced condensation of Q and T units, the total number of network bonds decreases with increasing substitution level. This general behaviour may be extended to our results on the physical and mechanical properties of the gels. Density values decrease from 1.84 (T100) to 1.29 g cm^{-3} (M100), as a result of a less well interconnected network. The same fact is observed for the E and ε_R values: these parameters are related to bond density and reflect increased network mobility as %MTES increases.[13,28] Linear shrinkage is maximum for T100 and decreases with increasing MTES content. Shrinkage may be ascribed to byproduct release and condensation between residual Si—OH groups after gel formation; the latter process is prominent in our case, owing to the experimental conditions employed. The possibility of affording a siloxane bond depends on the concentration of terminal Si—OH groups. Solid-state NMR spectra show that the M100 xerogel displays slow availability of Si—OH, since the T_2 units (OH and OEt terminal units) only amount to 12% and terminal silanols may be not present, in agreement with our ^{1}H MAS NMR and FTIR results. These facts and the hydrophobicity of sample M100,[29] preventing hydrolysis of residual Si—OR groups by adsorbed water, accounts for the absence of linear shrinkage observed in M100. In contrast, the shrinkage of T*x*M*y* xerogels increases with %TEOS, owing to the greater concentration of Si—OH groups and to the possible involvement of moisture to complete Si—OR hydrolysis.

Provincia Autonoma di Trento is greatly acknowledged for financial support.

References

1 H. Scholze, *J. Non-Cryst. Solids*, 1985, **73**, 669.
2 H. Schmidt, H. Scholze and G. Tunker, *J. Non-Cryst. Solids*, 1986, **80**, 557.
3 J. Wen, V. J. Vasudevan and G. L. Wilkes, *J. Sol–Gel Sci. Technol.*, 1995, **5**, 115.
4 P. Lacan, P. Le Gall, I. Rigola, C. Lurin, D. Wettling, C. Guizard and L. Cot, *Sol–Gel Optics II*, Proc. SPIE Vol. 1758, ed. J. D. Mackenzie, SPIE, Washington, DC, 1992, p. 464.
5 A. Kaiser, H. Schmidt and H. Bottner, *J. Membr. Sci.*, 1985, **22**, 257.
6 C. Guizard, N. Ajaka, M. P. Besland, A. Larbot and L. Cot, in *Polyimides and Other High Temperature Polymers*, ed. M. K. M. Abadie and B. Sillion, Elsevier, Amsterdam, 1991, p. 537.
7 C. Guizard and P. Lacan, in *Proc. 1st Eur. Workshop on Hybrid Organic Inorganic Materials*, Bierville, November 8–10, 1993, ed. C. Sanchez and F. Ribot, CNRS, Paris, 1993, p. 153.
8 T. Okui, Y. Saito, T. Okubo and M. Sadakata, *J. Sol–Gel Sci. Technol.*, 1995, **5**, 127.
9 S. Dirè, F. Babonneau, C. Sanchez and J. Livage, *J. Mater. Chem.*, 1992, **2**, 239.
10 Z. Zhang, Y. Tanigami, R. Terai and H. Wakabayashi, *J. Non-Cryst. Solids*, 1995, **189**, 212.
11 F. Babonneau, L. Bois, J. Maquet and J. Livage, in *Eurogel 91*, ed. S. Vilminot, R. Nass and H. Schmidt, Elsevier, Amsterdam, 1992, p. 319.
12 W. G. Fahrenholtz and D. M. Smith, *Mater. Res. Soc. Symp. Proc.*, 1992, **271**, 705.
13 H. H. Huang, B. Orler and G. Wilkes, *Macromolecules*, 1987, **20**, 1322.

14 Programs from Bruker Spectrospin, Wissembourg, France.
15 R. M. Almeida, T. A. Guitton and C. G. Pantano, *J. Non-Cryst. Solids*, 1990, **121**, 193.
16 F. Babonneau, K. Thorne and J. D. Mackenzie, *Chem. Mater.*, 1989, **1**, 554.
17 M. D. Sacks and R. Sheu, *J. Non-Cryst. Solids*, 1987, **92**, 383.
18 R. H. Glaser, G. L. Wilkes and C. E. Bronnimann, *J. Non-Cryst. Solids*, 1989, **113**, 73.
19 M. Mehring, *Principles of High Resolution NMR in Solids*, Springer-Verlag, Berlin, 1983, p. 129.
20 M. J. Muratagh, E. K. Graham and C. G. Pantano, *J. Am. Ceram. Soc.*, 1986, **69**, 775.
21 M. J. van Bommel, T. N. M. Bernards and A. H. Boonstra, *J. Non-Cryst. Solids*, 1991, **128**, 231.
22 (*a*) L. Delattre and F. Babonneau, *Mater. Res. Soc. Symp. Proc.*, 1994, **346**, 365; (*b*) S. Prabakar, R. A. Assink, N. K. Raman and C. J. Brinker, *Mater. Res. Soc. Symp. Proc.*, 1994, **346**, 979.
23 C. J. Brinker and G. W. Scherer, *Sol–Gel Science*, Academic Press, New York, 1990, ch. 3.
24 K. L. Walther, A. Wokaun and A. Baiker, *Mol. Phys.*, 1990, **71**, 769.
25 F. Babonneau, *Mater. Res. Soc. Symp. Proc.*, 1994, **346**, 949.
26 G. S. Carajava, D. E. Leyden, G. R. Quinting and G. E. Maciel, *Anal. Chem.*, 1988, **60**, 1776.
27 M. P. J. Peeters, W. J. J. Wakelkamp and A. P. M. Kentgens, *J. Non-Cryst. Solids*, 1995, **189**, 77.
28 R. H. Glaser and G. L. Wilkes, *Polym. Bull.*, 1988, **19**, 51.
29 C. Della Volpe, S. Dirè and E. Pagani, *J. Non-Cryst. Solids*, 1996, in press.

Paper 6/03554J; *Received* 21*st May*, 1996